Magnetostrophic balance as the optimal state for turbulent magnetoconvection

Eric M. King[a,1] and Jonathan M. Aurnou[b]

[a]Department of Earth and Planetary Science, University of California, Berkeley, CA 94720; and [b]Department of Earth, Planetary, and Space Sciences, University of California, Los Angeles, CA 90095

Edited by Peter L. Olson, Johns Hopkins University, Baltimore, MD, and approved December 12, 2014 (received for review September 18, 2014)

The magnetic fields of Earth and other planets are generated by turbulent convection in the vast oceans of liquid metal within them. Although direct observation is not possible, this liquid metal circulation is thought to be dominated by the controlling influences of planetary rotation and magnetic fields through the Coriolis and Lorentz forces. Theory famously predicts that planetary dynamo systems naturally settle into the so-called magnetostrophic state, where the Coriolis and Lorentz forces partially cancel, and convection is optimally efficient. Although this magnetostrophic theory correctly predicts the strength of Earth's magnetic field, no laboratory experiments have reached the magnetostrophic regime in turbulent liquid metal convection. Furthermore, computational dynamo simulations have as yet failed to produce a magnetostrophic dynamo, which has led some to question the existence of the magnetostrophic state. Here, we present results from the first, to our knowledge, turbulent, magnetostrophic convection experiments using the liquid metal gallium. We find that turbulent convection in the magnetostrophic regime is, in fact, maximally efficient. The experimental results clarify these previously disparate results, suggesting that the dynamically optimal magnetostrophic state is the natural expression of turbulent planetary dynamo systems.

rotating magnetoconvection | turbulence | planetary dynamos | stellar dynamos | magnetohydrodynamics

The magnetic fields of planets and stars are primary observable features that express the inner workings of these bodies, yet the detailed mechanics of their generation remains largely mysterious. It is generally accepted that the magnetic fields are generated within planetary and stellar interiors by turbulent motions of electrically conducting fluids through a process known as dynamo action. Convective stirring of such fluids (plasma in the sun, liquid iron alloys in the terrestrial planets and moons, metallized hydrogen in Jupiter and Saturn, and superionized water in Uranus and Neptune) is responsible for the magnetic fields we observe throughout the solar system (1). These natural dynamo systems exhibit complex variations over vast ranges of time and spatial scales, yet most of the dynamics responsible for the evolution of the magnetic fields are not directly observable. Earth's magnetic field, for example, is generated by convection occurring in the liquid metal outer core, which is isolated from geomagnetic observatories by the 2,900-km-thick mantle. Worse, the uppermost part of the mantle is magnetized, shielding all but the largest and slowest dynamics of the geodynamo from observation (2). Our understanding of the generation of the magnetic fields of Earth and other bodies, therefore, must rely heavily on magnetohydrodynamic theory, experiments, and simulations (3).

The theory of the geodynamo is largely concerned with the interactions among convection, magnetism, and rotation. The Earth's rotation period is about a million times shorter than the timescale for convective overturn in the core, and so core flow is strongly affected by the Coriolis force. The Coriolis force organizes turbulent convection and is ultimately responsible for the near alignment of the geomagnetic and geographic poles. In the limit of infinitely fast rotation, however, fluids suffer under the so-called Proudman–Taylor (P-T) constraint, and convection cannot occur at all. In the presence of an infinitely strong, uniform magnetic field, a similar constraint applies. Linear theory investigating the onset of convective instability has shown, however, that acting in unison, these two strong constraints can offset one another. In the limit of fast rotation, the presence of magnetic fields can relax the P-T constraint, and convection occurs most easily if Lorentz and Coriolis forces are similar in strength (4, 5).

The discovery of this magnetorelaxation process was quickly extrapolated from linear stability to fully developed turbulent convection and planetary dynamos (6, 7). Because the absolute magnitude of a dynamo-generated magnetic field is self-selected, it is widely assumed that the rapidly rotating planetary and stellar dynamos naturally settle into this optimal convective state, known as the magnetostrophic regime, in which Lorentz and Coriolis forces balance. One can estimate the relative strengths of these two forces using the Elsasser number, $\Lambda = \sigma B^2/(2\rho\Omega)$, where σ is the fluid's electrical conductivity, B is the magnetic field strength, ρ is the fluid density, and Ω is the planetary rotation rate. A dynamo in magnetostrophic balance has $\Lambda = O(1)$, such that magnetic field generation saturates, where $B^2 \propto \Omega$. Observational estimates for the geodynamo, for example, fall in the range $0.1 < \Lambda < 10$ (3, 8), substantiating the expectation that the geodynamo operates in a magnetostrophic regime.

To date, however, there exists no experimental evidence that magnetorelaxation can occur in turbulent liquid metal convection. Furthermore, numerical dynamo simulations, which have become the predominant method for examining planetary dynamo processes, have not yet produced a magnetostrophic dynamo, which indicates that either numerical modeling or the magnetostrophic theory is wrong (3).

Significance

What sets the strength of a planet's magnetic field? Theory suggests that there exists a "sweet spot" for magnetic field generation, in which the constraining influences of the Coriolis force (from planetary rotation) and Lorentz force (from the magnetic field) partially cancel, and the convective flow that generates magnetic energy is maximally efficient. However, this predicted optimal state, termed the magnetostrophic regime, has not yet been observed in computational dynamo simulations and has never been tested in a real, turbulent liquid metal, and so its existence has recently been called into question. Here, we report the first-ever, to our knowledge, turbulent magnetostrophic convection experiments. We observe that the magnetostrophic regime is, in fact, maximally efficient, substantiating the application of magnetostrophic theory to planets.

Author contributions: E.M.K. and J.M.A. designed research; E.M.K. and J.M.A. performed research; E.M.K. analyzed data; and E.M.K. and J.M.A. wrote the paper.

The authors declare no conflict of interest.

This article is a PNAS Direct Submission.

[1]To whom correspondence should be addressed. Email: ericmking@gmail.com.

This article contains supporting information online at www.pnas.org/lookup/suppl/doi:10.1073/pnas.1417741112/-/DCSupplemental.

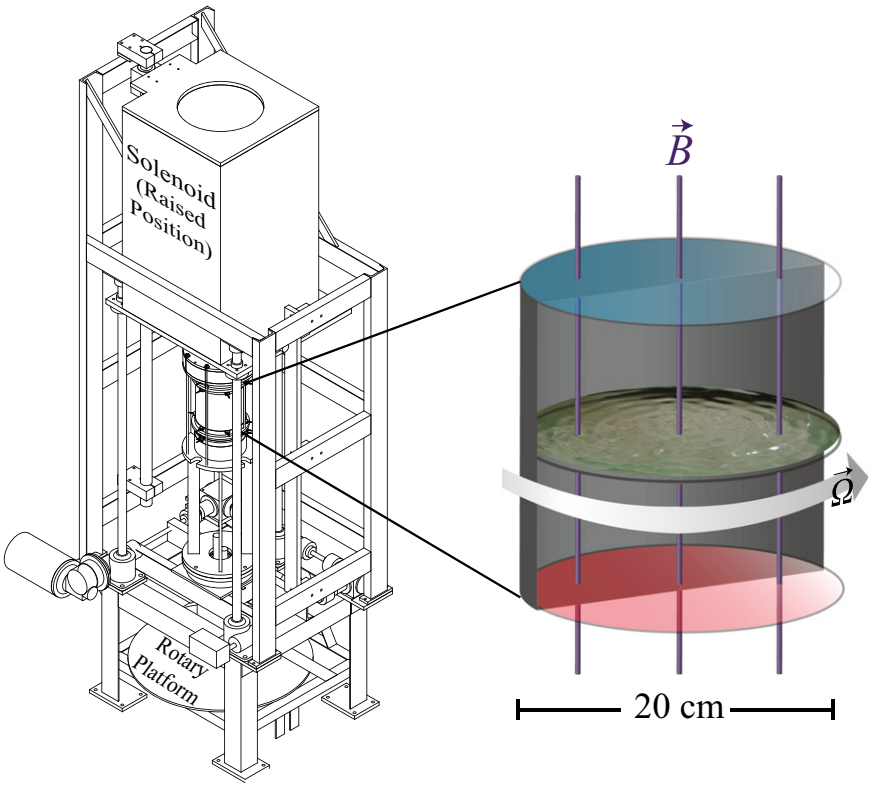

Fig. 1. Schematic representation of the experimental apparatus. Turbulent, rotating magnetoconvection is accomplished in the laboratory by applying a heat source to the base of a 20-cm cylinder filled with liquid gallium that is rotating at an angular rate Ω about a vertical axis within the center bore of a solenoidal electromagnet, which imposes a uniform vertical magnetic field, *B*.

Methods

Here, we show results from experiments in turbulent, rotating, liquid metal convection in the presence of strong, imposed magnetic fields. This setup, illustrated in Fig. 1, models the fluid dynamics of a local "piece" of a planetary dynamo, where convective instabilities dominate and the magnetic field is smooth enough to be considered externally imposed (9). Rotating magnetoconvection experiments have been conducted previously, but have thus far failed to be both turbulent and magnetostrophic. Nakagawa (10) examines the onset of plane layer rotating magnetoconvection in mercury. Aurnou and Olson (11) measure heat transfer by rotating magnetoconvection in gallium. The experiments of Nakagawa find that convection occurs most easily when $\Lambda = O(1)$, in support of the linear stability analysis, but Aurnou and Olson (11) find no evidence of magnetorelaxation. Neither study, however, drives convection to a turbulent state. Numerical simulations of rotating magnetoconvection have also revealed mixed results, but use unrealistic fluid properties and are similarly limited to nonturbulent states (e.g., refs. 12–15). Liquid metal magnetoconvection experiments in rotating spherical shells by Shew and Lathrop (16) and Gillet and colleagues (17) produce turbulent states, but the imposed magnetic fields are not strong enough to reach $\Lambda = O(1)$, and magnetorelaxation is not observed. Thus, the application of magnetostrophic theory to geophysically relevant, strongly nonlinear turbulence remains untested.

We investigate turbulent magnetostrophic convection, using a rotating horizontal layer of liquid gallium heated from below and with an imposed vertical magnetic field (Fig. 1). A cylindrical tank 20 cm in diameter and 20 cm in height is filled with the liquid metal gallium. The tank's sidewall is stainless steel, and on the top and bottom are thin layers of tungsten-coated copper. The liquid metal is heated from below by a noninductively wound electrical resistance element. Between 50 and 4,500 W are passed through the liquid gallium layer. This heat is removed by a thermostated heat exchanger above the working fluid volume. Temperature measurements are made near the top and bottom fluid surfaces by two arrays of six thermistors in the tank's top and bottom walls, 2 mm from the fluid. The convection tank is thermally insulated and rotated at up to 40 times per minute by a brushless servomotor. The magnetic field is imposed by a 450-kg solenoidal electromagnet. The magnet has a hollow 40-cm-diameter cylindrical inner bore and is held above the convection tank by a lift system, so the magnet can be lowered to surround the convection tank. The solenoidal coils are wound such that the magnet generates a vertical field up to 1,325 Gauss, uniform to within 0.5%. Heat flux *q* is measured as the input electrical power per unit area through the bottom surface of the container and is compared against measurements of the heat gains within the coolant circuit

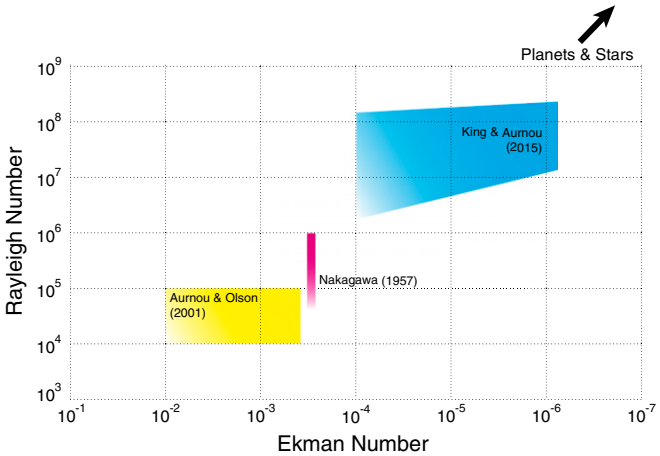

Fig. 2. Parameters accessed by magnetostrophic convection experiments. The strength of the Coriolis force is characterized by the inverse of the Ekman number, and the magnitude of thermal forcing is given by the Rayleigh number. Shown for comparison are the parameter values accessed by the experiments of Nakagawa (10), Aurnou and Olson (11), and the present study. Astrophysical and geophysical systems, such as the geodynamo, typically have $E < 10^{-10}$ and $Ra > 10^{20}$. A third dimensionless control parameter, not shown, is the strength of the Lorentz force, Λ.

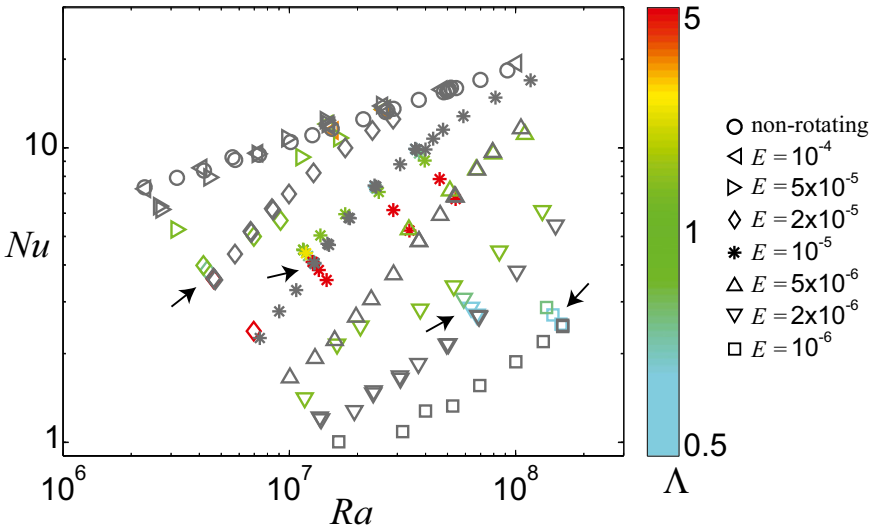

Fig. 3. Measurements of heat transfer efficiency, *Nu*, plotted versus *Ra*. Symbol shapes indicate rotation period *E*. Symbol color indicates magnetic field strength, Λ; gray symbols have $\Lambda = 0$. Nonrotating experiments with imposed magnetic fields are not shown because Λ would be undefined. Magnetic field strengths for the cases shown vary within the range $0 \le \Lambda \le 20$, but the color scale peaks at $\Lambda = 5$ for clarity near the magnetostrophic regime $\Lambda = O(1)$. Arrows indicate subsurveys explored in Fig. 4.

atop the convection tank. Heat flux measurement errors are tested by repeating experiments in the absence of convection (either by heating from the top or by replacing the liquid metal layer with a solid conductor) and by varying the mean temperature of the experiments relative to room temperature (by adjusting the coolant thermostat). Both the estimated measurement errors and temporal variation of the heat flux are less than ±5% for the present experiments. For more details on the experimental apparatus, see refs. 18–20.

Dimensionless characterization of the strength of thermal forcing is given by the Rayleigh number, $Ra = \alpha g \Delta T h^3/(\nu\kappa)$, where α is thermal expansivity, g is gravitational acceleration, ΔT is the temperature drop across the layer, h is the layer depth, ν is viscosity, and κ is thermal diffusivity. The Coriolis force is characterized by $E^{-1} = 2\Omega h^2/\nu$, where E is the Ekman number. The Prandtl number, $Pr = \nu/\kappa$, characterizes the diffusive properties of the fluid, and gallium has $Pr \approx 0.025$. Fig. 2 shows a comparison of the ranges of *Ra* and *E* accessed by the experiments with $\Lambda = O(1)$ of refs. 10 and 11 and the present study. The present experiments reach parameters more relevant to planets and stars, in that they produce more strongly driven convection (higher *Ra*) in the presence of stronger Coriolis forces (lower *E*) than the previous work. The geodynamo, for comparison, is thought to have $Ra \approx 10^{25}$ and $E \approx 10^{-15}$. Dimensionally, the experiments are then modeling roughly a 10^6 m^3 volume of the Earth's core.

The degree of turbulence in a given flow is usually quantified by its Reynolds number, $Re = UD/\nu$, where U is the typical flow speed and D is the length scale of interest. The threshold for the onset of turbulence generally occurs when $Re \gtrsim 1000$ (21). Because the present experiments are conducted in opaque liquid metal, we are unable to assess flow speeds by the usual optical methods. Scaling laws produced by previous convection studies, however, permit us to estimate *Re* using known quantities such as *Ra*. For example, the theoretical scaling laws of Cioni and colleagues (22) and King and colleagues (23), as well as the empirical scaling law of Yanagisawa (24), all predict that the present experiments have $10^3 \lesssim Re \lesssim 2 \times 10^4$, within the turbulent regime.

Results

We conducted 200 experiments across a range of the three independent control parameters: thermal driving, *Ra*; rotation period, *E*; and magnetic field strength, Λ. As the 3D parameter space is explored, the primary diagnostic of interest is the efficiency of convection, which is quantified using measurements of heat transfer. The Nusselt number measures the ratio of the total heat transfer to that by conduction alone, $Nu = qh/(k\Delta T)$, where q is the total heat flux and k is the thermal conductivity. Fig. 3 shows *Nu* versus *Ra* for the experiments, with *E* and Λ illustrated by symbol shape and color. All heat transfer data are also listed in Table S1.

For clarity, we focus our attention on four representative subsurveys, which are indicated by arrows in Fig. 3. For each subsurvey, we fix the rotation rate and heating rate and vary the magnetic field strength, Λ. We let Nu_0 represent the heat transfer efficiency for convection in the absence of magnetic fields, $\Lambda = 0$, to serve as a baseline for cases with $\Lambda > 0$. Fig. 4 shows how convective efficiency is affected by the imposition of magnetic fields of increasing strength. In it, we plot the relative efficiency, Nu/Nu_0, versus magnetic field strength, Λ, for each case. We observe that convection is maximally efficient when

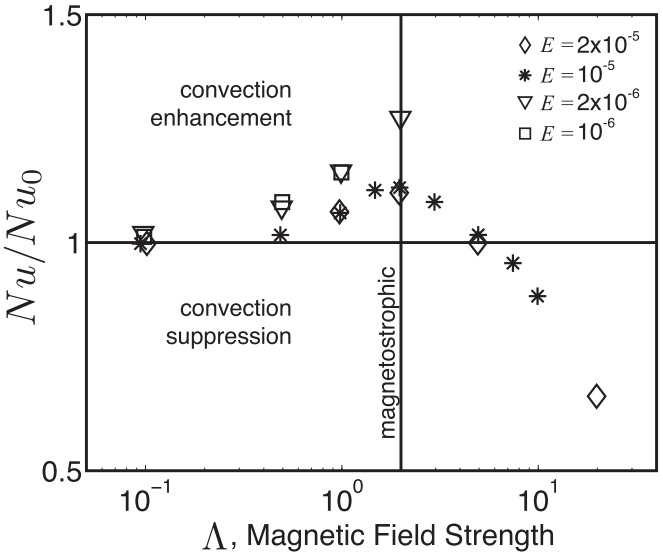

Fig. 4. Relative efficiency of heat transfer by convection (Nu/Nu_0) plotted versus Λ, the Elsasser number, which characterizes the relative strengths of Lorentz and Coriolis forces. Shown are cases with $Ra \approx 4.7 \times 10^6$ and $E = 2 \times 10^{-5}$ (◇), $Ra \approx 1.3 \times 10^7$ and $E = 10^{-5}$ (☆), $Ra \approx 7 \times 10^7$ and $E = 2 \times 10^{-6}$ (▽), and $Ra \approx 1.6 \times 10^8$ and $E = 10^{-6}$ (□). We observe that convection is maximally efficient in the magnetostrophic regime, where $\Lambda \approx 2$.

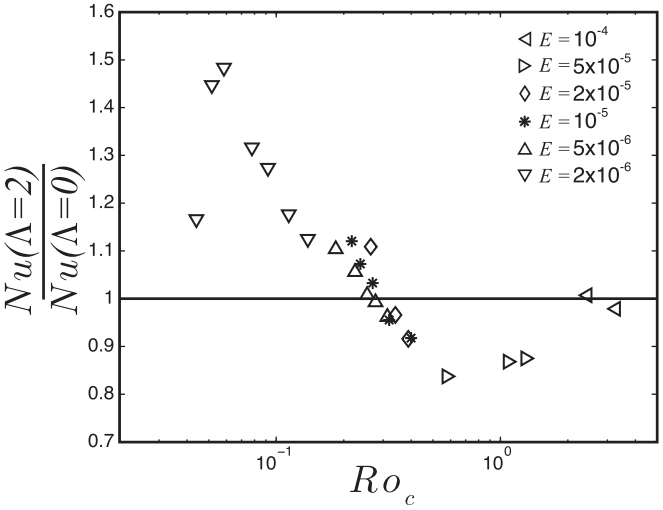

Fig. 5. Relative efficiency of heat transfer by magnetostrophic convection, $Nu(\Lambda=2)/Nu(\Lambda=0)$, is plotted versus the convective Rossby number, Ro_c, which characterizes the relative strengths of buoyancy and Coriolis forces. Symbol shapes represent E, as in Fig. 3. We observe that magnetostrophic convection is enhanced relative to nonmagnetic convection when $Ro_c \lesssim 0.25$.

$\Lambda = 2$, in agreement with the prediction of Chandrasekhar (4). This observation verifies that magnetorelaxation can occur in turbulent liquid metal convection. Similar results are found if the magnetic field strength is held fixed and the rotation rate is varied.

Discussion

Heuristically, Fig. 4 illustrates how the magnetostrophic state may be preferred in rapidly rotating planets and stars. When $\Lambda < O(1)$, Lorentz forces are either too weak to prevent field growth or actually promote the convective flow from which electromagnetic energy is derived, and so Λ increases. When $\Lambda > O(1)$, Lorentz forces suppress convection and inhibit the system's capacity for further field growth, and so Λ decreases, so that the system may naturally settle into the magnetostrophic state, $\Lambda = O(1)$. Our experiments therefore confirm that turbulent convection can be maximally efficient in the magnetostrophic regime. This result substantiates the extrapolation of magnetostrophic theory to turbulent geophysical and astrophysical systems, such as the geodynamo, as well as rapidly rotating stars (25–27, e.g.).

Fig. 3 also shows, however, that the magnetorelaxation effect occurs only when E and Ra are sufficiently small. As Ra and E increase, it is likely that inertial effects become comparable to the Coriolis and Lorentz forces, such that the magnetostrophic balance is no longer attained (e.g., refs. 28, 29). The competition between Coriolis and inertial effects is characterized by the convective Rossby number, $Ro_c = \sqrt{RaE^2/Pr}$. In Fig. 5, we isolate cases with $\Lambda = 2$ and plot their heat transfer relative to corresponding nonmagnetic experiments as a function of Ro_c. We find that experiments with $\Lambda = 2$ are enhanced relative to those with $\Lambda = 0$ when $Ro_c \lesssim 0.25$. In cases with $Ro_c \gtrsim 0.25$, we observe that magnetic fields instead suppress convection. This transition indicates that the system leaves the magnetostrophic regime when inertial effects become important.

This transition to inertially dominated convection is not likely to be important for planets such as Earth and Jupiter, where Coriolis forces are thought to be orders of magnitude stronger than inertial effects (8). Thus, if the results observed here hold as E is reduced further (even as Ra increases), the experiments suggest that magnetic fields will enhance the convection from which they are generated in these planets. However, in a broad range of stars, including sun-like stars, inertia and rotation play nearly equal roles (30). In these natural settings, our results suggest that strong magnetic fields will suppress convection.

The experimental observation of the magnetorelaxation effect stands in apparent contrast with recent studies of numerical dynamo simulations, in which the magnetostrophic state is not observed. Mean magnetic field strengths, which are outputs of each simulation, do not tend strongly toward $\Lambda = O(1)$. Scaling analysis for a wide array of numerical simulations suggests that it is buoyant power production, and not the rotation rate, that sets the saturation strength of the magnetic field (31, 32). A detailed look shows that Lorentz forces have only a minor affect on convection in such dynamo simulations (33). Further analysis suggests that the weak dynamic role of magnetic fields is owed to the unrealistically viscous fluids used by the simulations (34). In contrast, the present experimental study shows that turbulent rotating convection in a realistic fluid is enhanced by large-scale magnetic fields when $\Lambda = O(1)$ and is otherwise suppressed. Our results suggest that the magnetostrophic regime may in fact be the natural, optimal state for rapidly rotating convective dynamos.

ACKNOWLEDGMENTS. Support for laboratory experiment fabrication was provided by the US National Science Foundation Instrumentation & Facilities Program. E.M.K. acknowledges the support of the Miller Institute for Basic Research in Science. J.M.A. acknowledges the support of the US National Science Foundation Geophysics Program.

1. Stanley S, Glatzmaier GA (2010) Dynamo models for planets other than Earth. *Space Sci Rev* 152:617–649.
2. Finlay CC, Dumberry M, Chulliat A, Pais MA (2010) Short timescale core dynamics: Theory and observations. *Space Sci Rev* 155:177–218.
3. Roberts PH, King EM (2013) On the genesis of the Earth's magnetism. *Rep Prog Phys* 76(9):096801.
4. Chandrasekhar S (1954) The instability of a layer of fluid heated below and subject to the simultaneous action of a magnetic field and rotation. *Proc R Soc Lond A Math Phys Sci* 225:173–184.
5. Eltayeb IA (1972) Hydromagnetic convection in a rapidly rotating fluid layer. *Proc R Soc Lond* 326:229–254.
6. Eltayeb IA, Roberts PH (1970) On the hydromagnetics of rotating fluids. *Astrophys J* 162:669–701.
7. Stevenson DJ (1979) Turbulent thermal convection in the presence of rotation and a magnetic field: A heuristic theory. *Geophys Astrophys Fluid Dyn* 12:139–169.
8. Schubert G, Soderlund K (2011) Planetary magnetic fields: Observations and models. *Phys Earth Planet Inter* 187:92–108.
9. Braginsky and Meytlis (1990) Local turbulence in the Earth's core. *Geophys Astro Fluid* 55(2):71–87.
10. Nakagawa Y (1957) Experiments on the instability of a layer of mercury heated below and subject to the simultaneous action of a magnetic field and rotation. *Proc R Soc Lond A Math Phys Sci* 242:81–88.
11. Aurnou JM, Olson PL (2001) Experiments on Rayleigh-Bénard convection, magnetoconvection and rotating magnetoconvection in liquid gallium. *J Fluid Mech* 420: 283–307.
12. Zhang K, Schubert G (2000) Magnetohydrodynamics in rapidly rotating spherical systems. *Annu Rev Fluid Mech* 32:409–443.
13. Stellmach S, Hansen U (2004) Cartesian convection driven dynamos at low Ekman number. *Phys Rev E Stat Nonlin Soft Matter Phys* 70(5 Pt 2):056312.
14. Giesecke A (2007) Anisotropic turbulence in weakly stratified rotating magnetoconvection. *Geophys J Int* 171:1017–1028.
15. Varshney H, Baig MF (2008) Rotating magneto-convection: Influence of vertical magnetic field. *J Turbul* 9(33):1–20.
16. Shew W, Lathrop DP (2005) Liquid sodium model of geophysical core convection. *Phys Earth Planet Inter* 153:136–149.
17. Gillet N, Brito D, Jault D, Nataf H-C (2007) Experimental and numerical studies of magnetoconvection in a rapidly rotating spherical shell. *J Fluid Mech* 580:123–143.
18. King EM, Aurnou JM (2012) Thermal evidence for Taylor columns in turbulent rotating Rayleigh-Bénard convection. *Phys Rev E Stat Nonlin Soft Matter Phys* 85(1 Pt 2):016313.
19. King EM, Stellmach S, Aurnou JM (2012) Heat transfer by rapidly rotating Rayleigh-Bénard convection. *J Fluid Mech* 691:568–582.
20. King EM, Aurnou JM (2013) Turbulent convection in liquid metal with and without rotation. *Proc Natl Acad Sci USA* 110(17):6688–6693.

21. Davidson PA (2004) *Turbulence: An Introduction for Scientists and Engineers* (Oxford University Press, Oxford), p 661.
22. Cioni S, Ciliberto S, Sommeria J (1997) Strongly turbulent Rayleigh-Bénard convection in mercury: Comparison with results at moderate Prandtl number. *J Fluid Mech* 335:111–140.
23. King EM, Stellmach S, Buffett BA (2013) Scaling behavior in Rayleigh-Bénard convection with and without rotation. *J Fluid Mech* 717:449–471.
24. Yanagisawa T, et al. (2010) Detailed investigation of thermal convection in a liquid metal under a horizontal magnetic field: Suppression of oscillatory flow observed by velocity profiles. *Phys Rev E Stat Nonlin Soft Matter Phys* 82(5 Pt 2):056306.
25. Baliunas S, Sokoloff D, Soon W (1996) Magnetic field and rotation in lower main-sequence stars: An empirical time-dependent magnetic Bode's relation? *Astrophys J* 457:L99–L102.
26. Featherstone NA, Browning MK, Brun AS, Toomre J (2009) Effects of fossil magnetic fields on convective core dynamos in A-type stars. *Astrophys J* 705:1000–1018.
27. Morin J, Dormy E, Schrinner M, Donati J-F (2011) Weak- and strong-field dynamos: From the Earth to the stars. *Mon Not R Astron Soc* 418:L133–L137.
28. Sreenivasan B, Jones CA (2006) The role of inertia in the evolution of spherical dynamos. *Geophys J Int* 164:467–476.
29. Sreenivasan B, Jones CA (2011) Helicity generation and subcritical behaviour in rapidly rotating dynamos. *J Fluid Mech* 688:5–30.
30. Schrinner M, Petitdemange L, Dormy E (2012) Dipole collapse and dynamo waves in global direct numerical simulations. *Astrophys J* 752:121.
31. Christensen UR, Aubert J (2006) Scaling properties of convection-driven dynamos in rotating spherical shells and application to planetary magnetic fields. *Geophys J Int* 166:97–114.
32. Christensen UR (2011) Geodynamo models: Tools for understanding properties of Earth's magnetic field. *Phys Earth Planet Inter* 187:157–169.
33. Soderlund KM, King EM, Aurnou JM (2012) The influence of magnetic fields in planetary dynamo models. *Earth Planet Sci Lett* 333-334:9–20.
34. King EM, Buffett BA (2013) Flow speeds and length scales in geodynamo models: The role of viscosity. *Earth Planet Sci Lett* 371:156–162.

Pr	E	Ra	Ch	Nu
0.0245	∞	2.42×10^6	0	7.1
0.0244	∞	3.37×10^6	0	7.64
0.0244	∞	4.43×10^6	0	8.1
0.0241	∞	6.08×10^6	0	8.8
0.0242	∞	7.76×10^6	0	9.16
0.0241	∞	1.07×10^7	0	10.1
0.024	∞	1.34×10^7	0	10.7
0.0238	∞	1.63×10^7	0	11.2
0.0242	∞	2.24×10^7	0	12.1
0.0236	∞	2.86×10^7	0	12.9
0.0243	∞	2.81×10^7	0	12.8
0.0218	∞	3.02×10^7	0	13.1
0.0238	∞	3.93×10^7	0	14.1
0.0219	∞	5.26×10^7	0	15.1
0.0234	∞	5.06×10^7	0	14.9
0.0224	∞	5.21×10^7	0	15
0.0215	∞	5.3×10^7	0	15.3
0.0208	∞	5.39×10^7	0	15.4
0.0198	∞	5.64×10^7	0	15.4
0.0216	∞	7.3×10^7	0	16.4
0.0202	∞	9.52×10^7	0	17.7
0.0245	1.02×10^{-4}	2.45×10^6	0	7.02
0.0244	1.02×10^{-4}	4.33×10^6	0	8.27
0.0243	1.02×10^{-4}	7.64×10^6	0	9.27
0.0239	9.99×10^{-5}	1.59×10^7	0	11.5
0.0238	9.94×10^{-5}	2.8×10^7	0	13.1
0.0233	9.76×10^{-5}	4.96×10^7	0	15.2
0.0195	8.18×10^{-5}	1.04×10^8	0	18.8
0.0245	5.13×10^{-5}	2.87×10^6	0	5.97
0.0244	5.09×10^{-5}	4.67×10^6	0	7.68
0.0244	5.09×10^{-5}	7.62×10^6	0	9.22
0.024	5.02×10^{-5}	1.55×10^7	0	11.6
0.0239	5×10^{-5}	2.7×10^7	0	13.5
0.0245	2.05×10^{-5}	4.97×10^6	0	3.44
0.0244	2.04×10^{-5}	6.08×10^6	0	4.21
0.0243	2.03×10^{-5}	7.18×10^6	0	4.99
0.0241	2.02×10^{-5}	8.96×10^6	0	5.94
0.0242	2.02×10^{-5}	1.05×10^7	0	6.74
0.0242	2.02×10^{-5}	1.35×10^7	0	7.95

continued on next page

Pr	E	Ra	Ch	Nu
0.024	2.01×10^{-5}	1.86×10^{7}	0	9.66
0.024	2×10^{-5}	2.46×10^{7}	0	11.1
0.0237	1.98×10^{-5}	3.03×10^{7}	0	12.1
0.0243	1.02×10^{-5}	7.82×10^{6}	0	2.19
0.0242	1.01×10^{-5}	9.53×10^{6}	0	2.69
0.0241	1.01×10^{-5}	1.13×10^{7}	0	3.18
0.0239	9.99×10^{-6}	1.36×10^{7}	0	3.93
0.0239	1×10^{-5}	1.58×10^{7}	0	4.53
0.0239	1×10^{-5}	1.95×10^{7}	0	5.57
0.0238	9.96×10^{-6}	2.55×10^{7}	0	7.13
0.0236	9.87×10^{-6}	3.25×10^{7}	0	8.5
0.0238	9.95×10^{-6}	3.85×10^{7}	0	9.52
0.0232	9.7×10^{-6}	4.54×10^{7}	0	10.4
0.0216	9.04×10^{-6}	4.17×10^{7}	0	9.54
0.0234	9.79×10^{-6}	5.03×10^{7}	0	11.1
0.023	9.64×10^{-6}	6.17×10^{7}	0	12.4
0.0213	8.92×10^{-6}	8.49×10^{7}	0	14.3
0.0193	8.1×10^{-6}	1.2×10^{8}	0	16.4
0.0243	5.07×10^{-6}	1.06×10^{7}	0	1.6
0.0241	5.04×10^{-6}	1.37×10^{7}	0	1.86
0.024	5.01×10^{-6}	1.67×10^{7}	0	2.15
0.0238	4.97×10^{-6}	2.08×10^{7}	0	2.58
0.0238	4.97×10^{-6}	2.43×10^{7}	0	2.95
0.0237	4.95×10^{-6}	3.04×10^{7}	0	3.59
0.0235	4.92×10^{-6}	3.94×10^{7}	0	4.65
0.0233	4.87×10^{-6}	4.88×10^{7}	0	5.71
0.0232	4.85×10^{-6}	5.65×10^{7}	0	6.6
0.0242	2.02×10^{-6}	1.46×10^{7}	0	1.16
0.0242	2.02×10^{-6}	2.05×10^{7}	0	1.24
0.0243	2.03×10^{-6}	2.48×10^{7}	0	1.42
0.0243	2.03×10^{-6}	3.27×10^{7}	0	1.59
0.0241	2.01×10^{-6}	3.92×10^{7}	0	1.79
0.0236	1.97×10^{-6}	5.22×10^{7}	0	2.08
0.0228	1.91×10^{-6}	7.18×10^{7}	0	2.61
0.024	1×10^{-6}	1.74×10^{7}	0	0.972
0.024	1×10^{-6}	3.34×10^{7}	0	1.05
0.024	1×10^{-6}	4.22×10^{7}	0	1.24
0.0233	9.76×10^{-7}	5.54×10^{7}	0	1.29
0.0231	9.64×10^{-7}	7.3×10^{7}	0	1.51
0.0221	9.27×10^{-7}	1.05×10^{8}	0	1.82

continued on next page

Pr	E	Ra	Ch	Nu
0.0215	9.02×10^{-7}	1.38×10^{8}	0	2.13
0.0209	8.77×10^{-7}	1.68×10^{8}	0	2.39
0.0246	∞	2.37×10^{6}	9.46×10^{3}	7.23
0.0245	∞	3.3×10^{6}	9.5×10^{3}	7.78
0.0244	∞	4.32×10^{6}	9.54×10^{3}	8.31
0.0242	∞	5.95×10^{6}	9.6×10^{3}	8.94
0.0243	∞	7.53×10^{6}	9.58×10^{3}	9.42
0.0243	∞	1.06×10^{7}	9.58×10^{3}	10.2
0.0239	∞	2.8×10^{7}	9.74×10^{3}	13
0.0231	∞	5.08×10^{7}	1.01×10^{4}	15
0.0245	∞	3.1×10^{6}	4.68×10^{4}	5.52
0.0244	∞	4.11×10^{6}	4.7×10^{4}	6.24
0.0244	∞	5.13×10^{6}	4.72×10^{4}	6.99
0.0242	∞	6.81×10^{6}	4.75×10^{4}	7.81
0.0242	∞	8.44×10^{6}	4.74×10^{4}	8.4
0.0245	∞	3.81×10^{6}	9.35×10^{4}	4.5
0.0244	∞	5.02×10^{6}	9.39×10^{4}	5.11
0.0243	∞	6.33×10^{6}	9.43×10^{4}	5.67
0.0241	∞	8.25×10^{6}	9.49×10^{4}	6.46
0.0242	∞	1.01×10^{7}	9.48×10^{4}	7.05
0.0242	∞	1.33×10^{7}	9.47×10^{4}	8.11
0.0241	∞	1.89×10^{7}	9.53×10^{4}	9.56
0.023	∞	5.4×10^{7}	9.96×10^{4}	14.1
0.0245	∞	5.23×10^{6}	2.8×10^{5}	3.27
0.0244	∞	6.7×10^{6}	2.81×10^{5}	3.83
0.0242	∞	8.37×10^{6}	2.83×10^{5}	4.28
0.0241	∞	1.09×10^{7}	2.85×10^{5}	4.89
0.0241	∞	1.34×10^{7}	2.85×10^{5}	5.29
0.0244	∞	7.39×10^{6}	9.35×10^{5}	2.31
0.0243	∞	9.8×10^{6}	9.4×10^{5}	2.61
0.0241	∞	1.23×10^{7}	9.46×10^{5}	2.91
0.0239	∞	1.59×10^{7}	9.54×10^{5}	3.37
0.0239	∞	1.9×10^{7}	9.54×10^{5}	3.76
0.0238	∞	2.53×10^{7}	9.57×10^{5}	4.29
0.0236	∞	3.48×10^{7}	9.67×10^{5}	5.25
0.0223	∞	8.85×10^{7}	1.02×10^{6}	8.84
0.0185	∞	1.7×10^{8}	1.24×10^{6}	11.9
0.0242	∞	5.93×10^{6}	0	8.98
0.0239	∞	1.61×10^{7}	9.9×10^{5}	3.31
0.0237	9.9×10^{-5}	1.57×10^{7}	0	11.6

continued on next page

Pr	E	Ra	Ch	Nu
0.0237	9.9×10^{-5}	1.56×10^{7}	1.99×10^{4}	11.7
0.0237	9.9×10^{-5}	1.64×10^{7}	3.89×10^{4}	11.1
0.0239	9.99×10^{-5}	2.72×10^{7}	0	13.4
0.0239	9.99×10^{-5}	2.77×10^{7}	1.97×10^{4}	13.1
0.0239	9.98×10^{-5}	2.78×10^{7}	3.85×10^{4}	13.1
0.0245	5.13×10^{-5}	2.8×10^{6}	0	6.13
0.0245	5.12×10^{-5}	3.34×10^{6}	3.75×10^{4}	5.13
0.0243	5.07×10^{-5}	1.03×10^{7}	0	10.4
0.0242	5.06×10^{-5}	1.19×10^{7}	3.8×10^{4}	9.04
0.0237	4.96×10^{-5}	1.52×10^{7}	0	12
0.0237	4.94×10^{-5}	1.74×10^{7}	3.89×10^{4}	10.5
0.0245	2.04×10^{-5}	4.89×10^{6}	0	3.5
0.0245	2.05×10^{-5}	4.9×10^{6}	4.94×10^{3}	3.49
0.0245	2.05×10^{-5}	4.58×10^{6}	4.73×10^{4}	3.73
0.0245	2.05×10^{-5}	4.41×10^{6}	9.54×10^{4}	3.88
0.0245	2.05×10^{-5}	4.89×10^{6}	2.4×10^{5}	3.49
0.0244	2.04×10^{-5}	7.36×10^{6}	9.68×10^{5}	2.32
0.0243	2.03×10^{-5}	7.12×10^{6}	0	5.03
0.0243	2.03×10^{-5}	7.36×10^{6}	9.62×10^{4}	4.86
0.0241	2.02×10^{-5}	8.85×10^{6}	0	6.01
0.0241	2.01×10^{-5}	9.65×10^{6}	9.69×10^{4}	5.51
0.024	1×10^{-5}	1.36×10^{7}	0	3.92
0.024	1×10^{-5}	1.36×10^{7}	9.38×10^{3}	3.91
0.024	1×10^{-5}	1.34×10^{7}	4.83×10^{4}	3.98
0.024	1×10^{-5}	1.28×10^{7}	9.73×10^{4}	4.17
0.024	1×10^{-5}	1.22×10^{7}	1.46×10^{5}	4.37
0.024	1×10^{-5}	1.22×10^{7}	1.95×10^{5}	4.39
0.024	1×10^{-5}	1.25×10^{7}	2.94×10^{5}	4.26
0.024	1×10^{-5}	1.34×10^{7}	4.92×10^{5}	3.98
0.0239	1×10^{-5}	1.43×10^{7}	7.4×10^{5}	3.74
0.0239	9.99×10^{-6}	1.54×10^{7}	9.89×10^{5}	3.46
0.024	1×10^{-5}	1.55×10^{7}	0	4.57
0.024	1×10^{-5}	1.45×10^{7}	1.95×10^{5}	4.9
0.024	1×10^{-5}	1.93×10^{7}	0	5.6
0.024	1×10^{-5}	1.86×10^{7}	1.95×10^{5}	5.78
0.0239	1×10^{-5}	2.51×10^{7}	0	7.2
0.0239	1×10^{-5}	2.52×10^{7}	9.39×10^{3}	7.15
0.024	1×10^{-5}	2.52×10^{7}	4.84×10^{4}	7.16
0.0239	1×10^{-5}	2.55×10^{7}	9.76×10^{4}	7.07
0.0239	1×10^{-5}	2.62×10^{7}	1.96×10^{5}	6.88

continued on next page

Pr	E	Ra	Ch	Nu
0.0238	9.94×10^{-6}	3.04×10^{7}	4.96×10^{5}	5.98
0.0236	9.88×10^{-6}	3.58×10^{7}	1.00×10^{3}	5.09
0.0239	9.98×10^{-6}	3.8×10^{7}	0	9.59
0.0237	9.9×10^{-6}	3.8×10^{7}	9.49×10^{3}	9.64
0.0237	9.89×10^{-6}	3.84×10^{7}	4.9×10^{4}	9.55
0.0236	9.88×10^{-6}	3.94×10^{7}	9.89×10^{4}	9.31
0.0236	9.85×10^{-6}	4.18×10^{7}	1.99×10^{5}	8.8
0.0234	9.77×10^{-6}	4.86×10^{7}	5.04×10^{5}	7.61
0.0231	9.68×10^{-6}	5.72×10^{7}	1.02×10^{6}	6.52
0.0234	4.9×10^{-6}	3.94×10^{7}	0	4.65
0.0235	4.92×10^{-6}	3.56×10^{7}	4×10^{5}	5.13
0.023	4.8×10^{-6}	5.71×10^{7}	0	6.58
0.023	4.82×10^{-6}	5.39×10^{7}	4.09×10^{5}	6.95
0.0225	4.71×10^{-6}	7.09×10^{7}	0	8.14
0.0225	4.71×10^{-6}	7.03×10^{7}	4.18×10^{5}	8.2
0.0225	4.71×10^{-6}	8.3×10^{7}	0	9.34
0.0225	4.71×10^{-6}	8.36×10^{7}	4.19×10^{5}	9.27
0.0208	4.36×10^{-6}	1.1×10^{8}	0	11.2
0.0207	4.35×10^{-6}	1.14×10^{8}	4.55×10^{5}	10.8
0.0227	1.9×10^{-6}	7.23×10^{7}	0	2.59
0.0227	1.9×10^{-6}	7.07×10^{7}	5.1×10^{4}	2.65
0.0228	1.91×10^{-6}	6.68×10^{7}	2.57×10^{5}	2.79
0.0229	1.92×10^{-6}	6.2×10^{7}	5.14×10^{5}	3
0.0231	1.93×10^{-6}	5.61×10^{7}	1.02×10^{6}	3.3
0.0242	2.02×10^{-6}	1.44×10^{7}	0	1.18
0.0242	2.02×10^{-6}	1.24×10^{7}	9.76×10^{5}	1.37
0.0237	1.98×10^{-6}	2.48×10^{7}	0	1.45
0.024	2×10^{-6}	1.71×10^{7}	9.87×10^{5}	2.09
0.0239	2×10^{-6}	3.25×10^{7}	0	1.62
0.0243	2.03×10^{-6}	2.18×10^{7}	9.74×10^{5}	2.41
0.0231	1.93×10^{-6}	5.3×10^{7}	0	2.09
0.0234	1.96×10^{-6}	3.99×10^{7}	1.01×10^{6}	2.75
0.0219	1.83×10^{-6}	1.06×10^{8}	0	3.68
0.0222	1.86×10^{-6}	8.88×10^{7}	1.06×10^{6}	4.33
0.0208	1.75×10^{-6}	1.56×10^{8}	0	5.28
0.0212	1.78×10^{-6}	1.37×10^{8}	1.12×10^{6}	5.94
0.0207	8.69×10^{-7}	1.68×10^{8}	0	2.42
0.0207	8.69×10^{-7}	1.68×10^{8}	1.08×10^{4}	2.41
0.0208	8.71×10^{-7}	1.65×10^{8}	1.13×10^{5}	2.45
0.021	8.8×10^{-7}	1.52×10^{8}	5.62×10^{5}	2.63

continued on next page

Pr	E	Ra	Ch	Nu
0.0212	8.87×10^{-7}	1.43×10^{8}	1.12×10^{6}	2.79

Table 1: Heat transfer data from rotating magnetoconvection experiments. $Pr = \nu/\kappa$, $E = \nu/2\Omega h^2$, $Ra = \alpha g \Delta T h^3/\nu\kappa$, $Ch = \sigma B^2 h^2/(\rho\nu) = \Lambda/E$ and $Nu = qh/k\Delta T$, where ν is the fluid's kinematic viscosity, κ is the fluid's thermal diffusivity, Ω is angular rotation rate, h is the height of the container, α is the fluid's thermal expansivity, g is gravitational acceleration, ΔT is the temperature drop across the convection tank, σ is electrical conductivity, B is the magnetic field strength, ρ is the fluid density, q is heat flux, and k is the fluid's thermal conductivity. Gallium is the working fluid and $h = 19.7$ cm for all cases.